Application of Uniform Strain Theory to Heterogeneous Granular Solids

Ching S. Chang, Anil Misra

Application of Uniform Strain Theory to Heterogeneous Granular Solids

By Ching S. Chang,[1] Member, ASCE, and Anil Misra,[2] Student Member, ASCE

Abstract: The micro- and the macro-mechanical measures of heterogeneous granular solids are investigated using two methods, namely a computer simulation method, and a micro-structural continuum method. The micro-structural continuum method used in this study is based on a uniform strain assumption. The applicability of the uniform strain assumption is evaluated by comparing the results from the micro-structural continuum method to those from the computer simulation method. Two types of granular solids, viz. with linear bonded contacts and with nonlinear frictional contacts, are studied to investigate the influence of contact behavior on the heterogeneity of the strain field. It is observed that packings with bonded contacts have a reasonably homogeneous strain field, implying that the uniform strain assumption is applicable for this condition. Packings with frictional contacts have a heterogeneous strain field, except at low levels of deviatoric stress. The natures of inhomogeneity for the particle rotation, stress, and contact force fields in granular solids are also discussed.

Introduction

The overall stress-strain behavior of a granular material is significantly influenced by the micro-scale interactions between the granules. Therefore, to characterize accurately stress and strain in granulates, one needs to formulate them in terms of the micro-scale measures of forces and deformations. A number of investigators have addressed various aspects of these fundamental problems—for example: packing structure measures, such as the spatial distribution of branch vectors (the vectors joining centroids of particles in contact) and of normal vectors at the inter-particle contacts, have been introduced (Oda 1972a; Oda et al. 1980); and the definitions of stress for granular materials in terms of inter-particle contact forces have been discussed by Christoffersen et al. (1981), Drescher and DeJong (1972), and a number of papers in Cowin and Satake (1978), Jenkins and Satake (1982), and Satake and Jenkins (1988).

Along this line of approach, efforts have been made to relate the stress and strain of granular media (Digby 1981; Walton 1987; Jenkins 1987; Chang 1987; Bathurst and Rothenburg 1988). Digby (1981) studied the effective elastic moduli of porous rocks by considering them to be composed of spherical particles bonded at particle contacts assuming that no shear force exists at the contact. Walton (1987) studied the moduli of isotropic packings of equal spheres under axisymmetrical loading considering both normal and shear compliances at the contact. Along the same lines, Jenkins (1987) investigated the volume change behavior of packings of equal spheres under small-strain axisymmetrical deformation, Bathurst and Rothenburg (1988) studied the behavior of disk packings with linear contact interactions, and Chang (1987) developed stress-strain relationships for regular and random packings of spheres. Results from these models have been reported to give encouraging agreement with experimental results on the moduli of regular packings and random packings of disks (Chang and Misra 1989a; Xue 1988) and volumetric strain of random packings of glass beads (Jenkins 1987). These comparisons have been conducted in the range of small strains only. However, because of some simplifying assumptions on the kinematics of the media, the aforementioned models are not expected to perform well at large strain levels. The three assumptions made in the aforementioned models are as follows: (1) The evolution of packing parameters with the loading process is neglected; (2) the particle centroids move in accordance with a uniform strain field; and (3) the particles' rotations are neglected (except in Chang 1987). Although the three factors are considered to be directly related to large strain problems, studies conducted by including the evolution of packing parameters and particle rotations show that the micro-structural model with a uniform strain assumption still gives a poor agreement at large strain levels (Chang and Misra 1989b). This implies that heterogeneity of the strain field is a significant factor influencing the stress-strain behavior of granular materials. At stress levels near failure, qualitative evidence of inhomogeneity in the strain field has also been observed from experiments on sands (Roscoe 1970) and rod assemblies (Oda 1972b). Therefore, it is desirable to evaluate the applicability of the uniform strain assumption in predicting the micro- and the macro-mechanical behavior of granular solids.

Due to the difficulty of measuring the movement of each particle during a deformation process, the micro-mechanical behavior of granular materials cannot be investigated using experimental methods. On the other hand, the computer simulation method (Cundall and Strack 1979) offers a viable way to study quantitatively the micro-mechanical behavior (e.g., the strain field, the stress field, particle rotations, and contact forces) of the granular materials. In this study, the computer simulation method is employed to simulate the stress-strain behavior of granular packings and to investigate the micro-mechanical behavior. The objective of this study is twofold: (1) To obtain the applicability range of the uniform strain assumption; and (2) to offer insight for further improvement of the micro-structural continuum model for near failure conditions. In this work, we compare the stress-strain behavior of packings obtained from the micro-structural continuum method (with uniform strain assumption) and that obtained from the computer simulation at various levels of deviatoric stress up to the failure conditions. We then discuss the uniformity of the strain field, the particle rotations field, and the stress field.

The comparisons are made for two types of contact interactions, namely bonded contacts with linear properties, and frictional contacts with nonlinear force-dependent properties. The bonded contacts do not include sliding or separation at the contacts, while the nonlinear contact allows for sliding as well as separation. Results show the strain field to be fairly uniform for packings with bonded contacts. For packings with frictional contacts, the strain field is found to be uniform at low levels of deviatoric stress but become increasingly heterogeneous at high levels of deviatoric stress. This has an implication for the applicability of the micro-structural continuum model

[1]Prof., Dept. of Civ. Engrg., Univ. of Massachusetts, Marston Hall, Amherst, MA 01003.

[2]Res. Asst., Dept. of Civ. Engrg., Univ. of Massachusetts, Marston Hall, Amherst, MA.

Note. Discussion open until March 1, 1991. To extend the closing date one month, a written request must be filed with the ASCE Manager of Journals. The manuscript for this paper was submitted for review and possible publication on August 8, 1989. This paper is part of the ***Journal of Engineering Mechanics***, Vol. 116, No. 10, October, 1990. ©ASCE, ISSN 0733-9399/90/0010-2310/$1.00 + $.15 per page. Paper No. 25118.

presented here for problems of packings with bonded granules and packings with frictional granules at low levels of deviatoric stresses.

Description of Granular System

The granular system is envisioned to be composed of rigid particles connected to each other at the particle contacts by deformable springs that account for the particle deformation at the inter-particle contacts. The deformation is assumed to be rate-independent and occurring under quasi-static conditions. Thus the forces and deformations originating from particle momentum and velocity are neglected in the analysis. The assembly deformation under an increment of load causes the particles in the assembly to move relative to each other. Considering each particle to have six degrees of freedom, namely three translational and three rotational degrees of freedom, the relative displacement $\Delta\delta_i$ at the contact of any two particles m and n is given by

$$\Delta\delta_i = \Delta u_i^m - \Delta u_i^n + e_{ijk}(\Delta\omega_j^m r_k^m - \Delta\omega_j^n r_k^n) \quad (1)$$

and the relative rotation $\Delta\theta_i$ at the contact is given by

$$\Delta\theta_i = \Delta\omega_i^m - \Delta\omega_i^n \quad (2)$$

where Δu_i = the particle displacement; $\Delta\omega_k$ = the particle rotation; r_j = the vector joining the centroid of a particle to the contact point; superscripts refer to the particles; and e_{ijk} = the permutation symbol.

This relative movement between particles is resisted by, in general, stretch springs and rotational springs at the contact. While the stretch springs resist the relative displacement between the two particles in contact, the rotational springs resist the relative rotation between contacts. The incremental relative displacement at the contact $\Delta\delta_j$ is related to the incremental contact force Δf_i as follows:

$$\Delta f_i = K_{ij}\Delta\delta_j \qquad (i, j = x, y, z) \quad (3)$$

where K_{ij} = the tangent contact stiffness tensor. Considering a simple case where the shear forces are uncoupled from the normal displacements and vice versa, Eq. 3 can be simplified to

$$K_{ij} = K_n n_i n_j + K_r(s_i s_j + t_i t_j) \quad (4)$$

where K_n and K_r = the tangent contact stiffnesses along the normal and tangential direction of the contact surface, respectively. The unit vector **n** is normal to the contact surface and vectors **s** and **t** are arbitrarily chosen such that **nst** forms a local Cartesian coordinate system. This simplified contact stiffness tensor is fairly reasonable for two elastic nonconforming bodies in contact (Mindlin and Deresiewicz 1953). The tangent contact stiffnesses K_n and K_r based on the Hertz-Mindlin theory of frictional contacts for: (1) A two-disk system; and (2) a two-sphere system are given in Appendix I. In a similar way, the incremental relative rotation at the contact $\Delta\theta_j$ is related to the incremental contact couple $\Delta\mu_i$ as follows:

$$\Delta\mu_i = G_{ij}\Delta\theta_j \qquad (i, j = x, y, z) \quad (5)$$

where G_{ij} = the rotational stiffness tensor. Again, considering the three components of the rotation to be uncoupled, Eq. 5 is simplified to

$$G_{ij} = G_n n_i n_j + G_r(s_i s_j + t_i t_j) \quad (6)$$

where G_n = the torsional stiffness at the contact; and G_r = the rolling stiffness. The micro-structural continuum model and the computer simulation method used in this work are based on this conceptual model of granular systems.

Constitutive Law for Granular Solid Based on Uniform Strain Theory

Based on the micro-structural continuum model with the uniform strain assumption, the relationship between incremental stress and the incremental overall strain for a granular material with a given packing structure can be written as (Chang 1987)

$$\Delta\sigma_{ij} = C_{ijkl}\Delta\epsilon_{kl} \quad (7)$$

where

$$C_{ijkl} = \frac{1}{2V}\sum_n\sum_m l_i^{nm}K_{jl}^{nm}l_k^{nm} \quad (8)$$

where V = the volume of the packing; and $l_j^{nm} = X_j^m - X_j^n$ = the branch vector joining the centroids of particles n and m in contact.

Strain

In Eq. 7, the incremental strain $\Delta\epsilon_{kl}$, is defined as

$$\Delta\epsilon_{kl} = \Delta u_{l,k} + e_{lkm}\Delta\omega_m \quad (9)$$

where $\Delta u_{l,k}$ = the incremental displacement gradient; and $\Delta\omega_m$ = the average incremental rotation of the particles in the packing. The usual strain increment tensor of conventional continuum mechanics is recovered by taking the symmetric part of the incremental strain tensor $\Delta\epsilon_{kl}$, given as

$$\Delta\epsilon_{(kl)} = \Delta u_{(l,k)} = \frac{1}{2}(\Delta u_{l,k} + \Delta u_{k,l}) \quad (10)$$

However, the skew-symmetric part does not equal the rigid body rotation as in the conventional definition. The skew-symmetric part of the incremental strain tensor $\Delta\epsilon_{kl}$, given by

$$\Delta\epsilon_{[kl]} = \Delta u_{[l,k]} + e_{lkm}\Delta\omega_m = \frac{1}{2}(\Delta u_{l,k} - \Delta u_{k,l}) + e_{lkm}\Delta\omega_m \quad (11)$$

represents the particle rotations in excess of the rigid body rotation $\Delta u_{[l,k]}$. Based on this definition of the incremental strain field $\Delta\epsilon_{ij}$, the incremental relative displacement $\Delta\delta_i^{nm}$ at the contact is defined in terms of the branch vector as

$$\Delta\delta_i^{nm} = \Delta\epsilon_{ji}l_j^{nm} \quad (12)$$

The incremental strain field is assumed to be uniform within the sample; that

is, the incremental relative displacements at all contacts are assumed to be compatible with a uniform overall incremental strain. Substituting Eq. 9 into Eq. 12 and comparing it to Eq. 1, it is seen that this definition of the incremental strain tensor $\Delta\epsilon_{ij}$ implies that an incremental load at a given instant will cause the particles in the assembly to displace and rotate in accordance with a linear incremental displacement field and a uniform incremental rotation field, respectively.

Stress

The incremental stress, $\Delta\sigma_{ij}$, is taken to be the volume average of the tensor product of the incremental contact force Δf_j^{nm} and the branch vector l_i^{nm}

$$\Delta\sigma_{ij} = \frac{1}{2V}\sum_n \sum_m l_i^{nm}\Delta f_j^{nm} \quad \ldots\ldots (13)$$

The incremental contact force Δf_j^{nm} is determined from the incremental relative displacement $\Delta\delta_i^{nm}$ at the contact based on the local constitutive law defined in Eq. 3.

Evolution

The incremental formulation of the stress-strain relationship discussed here is valid only for the case of infinitesimal deformations. During a loading process, however, it is necessary to account for the nonlinearity of the contact stiffness, and include the effect of evolution of the branch vector l_i and the packing volume V at end of each load increment.

The nonlinear Hertz-Mindlin contact stiffness (given in Appendix I) is governed by the contact forces. For this nonlinear contact interaction, the evolution of contact forces is governed by the following equation:

$$f_i = K_{ij}(\mathbf{f})\Delta\epsilon_{kj}l_k + f_i^o \quad \ldots\ldots (14)$$

where f_i^o = the contact force at the instant of loading. To account fully for the nonlinearity of the contact stiffness K_{ij}, an iterative procedure is employed within each increment until Eq. 14 is satisfied. During the loading process, when the normal force at a contact relaxes (i.e., $f_n \leq 0$) the contact becomes inactive; that is, the normal and the tangential contact stiffnesses vanish. At an active contact (i.e., $f_n > 0$), Coulomb's frictional law is assumed such that for tangential force at a contact $f_s > f_n \tan\phi_\mu$, sliding occurs and the contact does not carry any additional tangential force. During each loading step, any excess tangential force is converted to an unbalanced stress using Eq. 13 and applied back to the system. For the linear bonded contacts, Eq. 14 becomes exact and the mechanisms of inactivating contacts and contact sliding are not applied.

The evolution equation governing the change of the branch vector l_i over an increment of load is given by

$$l_i = (\Delta\epsilon_{ji} + \delta_{ij})l_j^o \quad \ldots\ldots (15)$$

where l_j^o = the branch vector at the instant of the incremental loading; and δ_{ij} = the Kronecker delta. The particle rotation $\Delta\omega_k$ can be obtained from the rigid body rotation, $\Delta u_{[i,j]}$, and the skew-symmetric part of incremental strain, $\Delta\epsilon_{[ij]}$. The evolution equation of the change of volume of the packing is written as

$$V = (\Delta\epsilon_{kk} + 1)V^o \quad \ldots\ldots (16)$$

where V^o = the volume at the instant of the loading.

Comparison of Micro-Structural Continuum Model and Computer Simulation

Packing and Loading Conditions

To evaluate the micro-structural continuum model based on uniform strain theory, we study the stress-strain behavior of random packings of disks and spheres and compare the results to those obtained from the computer simulation method. The computer simulation method employed in this work is briefly discussed in Appendix I. The two-dimensional (2-d) packings of disks and three-dimensional (3-d) packings of spheres used in the study are shown in Figs. 1(*a–c*), respectively. The particle size and number of particles, the total number of contacts, the coordination number, the area (for 2-d packings) or volume (for 3-d packings), and the void ratio of the three packings are given in Table 1. The total number of contacts N is obtained as $\Sigma_n C_n$, where C_n is the number of contacts for the nth particle and the summation is carried over all the particles.

Two types of contact interactions are used in this study: (1) Frictional contacts with nonlinear properties obtained from the Hertz-Mindlin contact theory (given in Appendix I); and (2) bonded contacts with linear properties. The frictional contact has force-dependent properties and allows for sliding as well as separation of the contact. The bonded contact, on the other hand, is independent of the contact forces and does not consider particle slip or

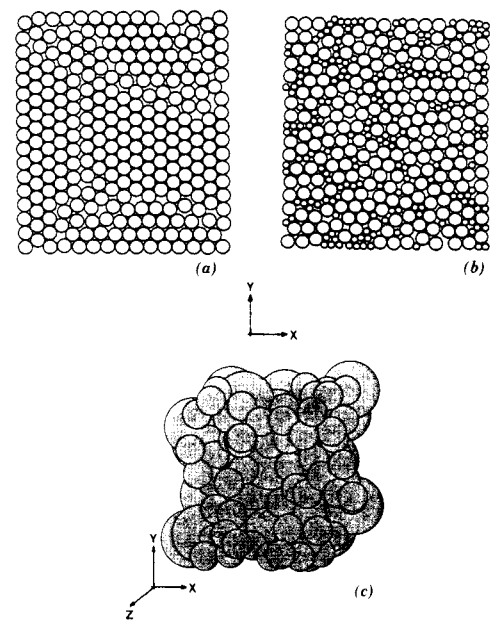

FIG. 1. Packings: (*a*) One-Size Disks (Packing A); (*b*) Two-Size Disks (Packing B); and (*c*) Spheres (Packing C)

TABLE 1. Packing Parameters for Three Packings

Parameter (1)	Packing A (2)	Packing B (3)	Packing C (4)
Particle diameter (number of particles)	12.7 mm (276)	12.7 mm (278) 6.35 mm (127)	0.6 mm (25) 0.3 mm (70)
Number of contacts	1,414	2,094	490
Coordination number	5.12	5.17	5.16
Area/volume	3.61×10^{-2} m^2	3.8×10^{-2} m^2	5.83×10^{-9} m^3
Void ratio	0.117	0.108	0.5

separation. For packings with bonded contacts, the contact stiffness is assumed to be the same for all the contacts in the packing. The particle shear modulus G_g, particle Poisson's ratio ν_g, and inter-particle friction angle ϕ_μ used for obtaining the stiffnesses K_n and K_s for the frictional contacts are given in Table 2. For the bonded contacts, the values of the stiffnesses K_n and K_s are also given in Table 2. It is noted that, for Hertz-Mindlin contact, the value of K_s is within the range of $0.66K_n$ to K_n when the contact shear force is absent. For the bonded contact, K_s is chosen to be $0.5K_n$ for the examples in Table 2. Other values of K_s ranging from $0.5K_n$ to K_n have been used and found to give similar results. Since only circular particles are considered, the area of contact between two particles is very small. Thus, the rotational stiffness G_{ij} is small and is neglected in this analysis.

The deformation behavior of the 2-d and 3-d packings are studied under biaxial compression and triaxial compression loading paths, respectively. For the 2-d case, the loading path is such that $\Delta\sigma_{yy} > 0$ and $\Delta\sigma_{xx} = \Delta\sigma_{xy} = \Delta\sigma_{yx} = 0$. For the 3-d case, the loading path is such that $\Delta\sigma_{zz} > 0$ and the increments of the other stress components are zero. The packings are first loaded to an initial isotropic stress state (17.25 kPa for 2-d packings and 69 kPa for 3-d packings) prior to the compression loading.

Stress-Strain Curves

The stress-strain curves of the 2-d packings A and B with bonded contacts and with frictional contacts are shown in Fig. 2(*a*). The stress-strain curve for the 3-d packing is shown in Fig. 2(*b*). In Figs. 2(*a* and *b*) the curves with no symbols are obtained from the micro-structural continuum model and the curves with symbols are obtained from the computer simulation method.

For packings with bonded contacts, the difference of the results from the micro-structural continuum and the computer simulation methods is within 10% at all levels of deviatoric stress. This discrepancy is expected to be due

TABLE 2. Parameters for Contact Stiffness

Packing (1)	Frictional Contact			Bonded Contact	
	G_g (2)	ν_g (3)	ϕ_μ (4)	K_n (5)	K_s (6)
A	2.1×10^6 kPa	0.1	15°	17.5×10^5 N/m	8.8×10^5 N/m
B	2.1×10^6 kPa	0.1	15°	17.5×10^5 N/m	8.8×10^5 N/m
C	29×10^6 kPa	0.2	15°	17.5×10^5 N/m	8.8×10^5 N/m

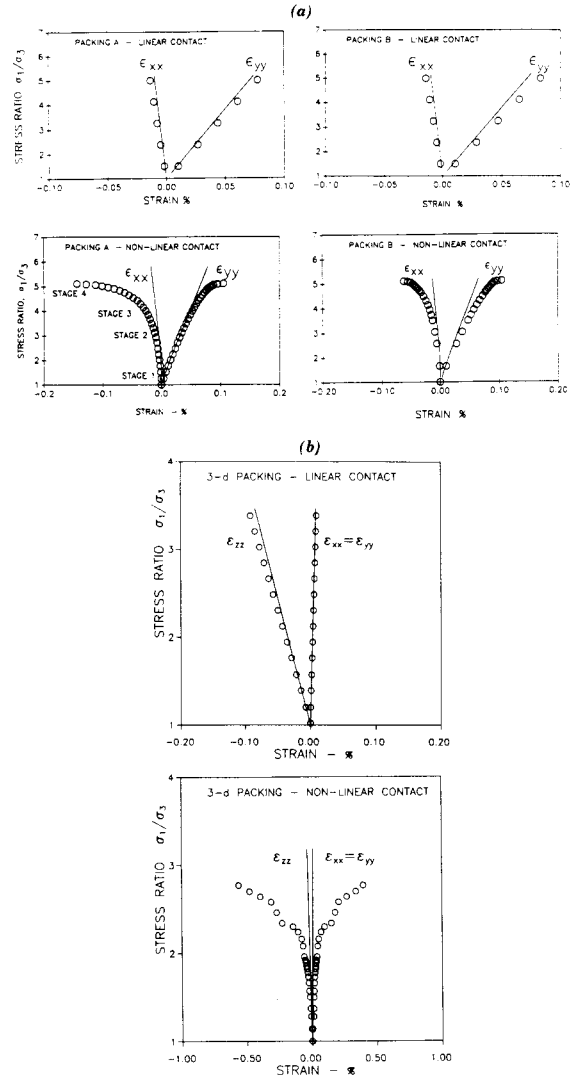

FIG. 2. Stress-Strain Behavior: (*a*) Packings A and B for Bonded and Frictional Contacts (Symbols = Uniform Strain Theory, Solid Line = Computer Simulation); and (*b*) Packing C for Bonded and Frictional Contacts (Symbols = Uniform Strain Theory, Solid Line = Computer Simulation)

to the inhomogeneity of the strain field introduced by the inhomogeneous nature of the packing structure. However, the close agreement of the results implies that the influence of packing structure on the inhomogeneity of strain field is small.

For packings with frictional contacts, the stress-strain curves obtained from the two methods match closely at low stress levels. For example, the initial

TABLE 3. Initial Moduli for 3-d Packing C

Moduli (1)	Uniform strain method (2)	Computer simulation (3)
E_{xx}	5.49×10^5 kPa	5.14×10^5 kPa
E_{yy}	5.39×10^5 kPa	5.63×10^5 kPa
E_{zz}	5.21×10^5 kPa	5.44×10^5 kPa
G_{xy}	2.68×10^5 kPa	2.59×10^5 kPa

moduli for the 3-d packing computed under the initial confining pressure based on the two methods are within 10% of each other, as shown in Table 3. However, at higher stress levels the stress-curves obtained from the two methods deviate rapidly. Note that the micro-structural continuum model used here incorporates the effect of packing evolution and particle rotations. Therefore, the major source of discrepancy is expected to be due to the heterogeneity of the field variables. At high stress levels, due to the increasing number of contacts experiencing sliding and separation, the strain field is expected to be highly heterogeneous. In contrast, at low stress levels with small amounts of sliding contacts, the strain field is expected to be uniform. Fig. 3(*a*) shows the fraction contacts sliding and lost for packing A with an increase of the deviatoric stresses. For the stress ratio of about 1.5, the number of contacts sliding are within 5% of the total contacts while no contact has been lost. As the stress ratio increases, the percentages of both contacts sliding and contacts lost increase. The directional distribution of the contacts

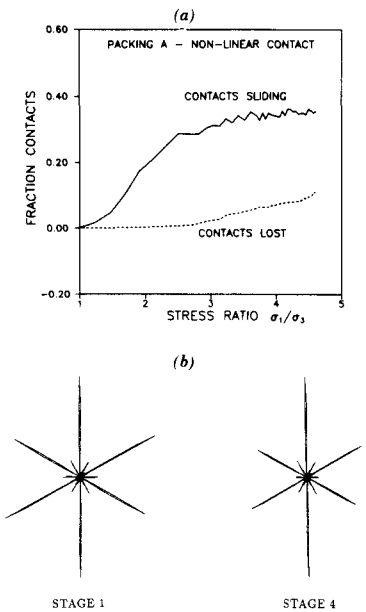

FIG. 3. Contacts: (*a*) Contacts Sliding and Lost for Packing A with Increasing Stress Ratio; and (*b*) Contact Normal Distributions for Packing A at Stages 1 and 4 of Stress-Strain Curve in Fig. 2

lost is seen from contact normal distribution of packing A at stages 1 and 4 of the stress-strain curve plotted in Fig. 3(*b*). With the increase of the deviatoric loading, the contacts along the minor principal direction continually disappear.

These comparisons imply that, although the packing structure is heterogeneous in nature, the micro-structural continuum model with a uniform strain assumption is applicable to predicting the stress-strain behavior for packings with bonded linear contacts. It also gives good agreement for packings with nonlinear frictional contacts at low stress levels (stress ratio ~1.5).

Variation of Micro-Mechanical Quantities in Packing

We next investigate the applicability of the micro-structural continuum model with a uniform strain assumption in predicting the various micro-mechanical quantities and their variation in the packing. We study the heterogeneity of the particle displacement, the particle rotation, the stress, and the contact force fields, at four loading stages marked in Fig. 2(*a*). The four stages are chosen to correspond to the initial isotropic loading (stage 1), the stress ratio at dilation (stage 3), the stress ratio intermediate between stage 1 and 3 (stage 2), and the stress ratio at failure (stage 4). The subsequent results are discussed for packing A only; however, similar behavior was found for the other packings as well.

Displacement Field in Packing

In order to study the nonlinearity of the incremental displacement field, the displacements of particle centroids obtained from the computer simulation, at each increment of the loading, are approximated by continuous linear functions using the least-squares method. The linear functions used are of the following form:

$$\overline{\Delta u_i}(X, Y) = a_i + b_i X + c_i Y \quad \ldots\ldots (17)$$

where $\overline{\Delta u_i}(X, Y)$ = the displacement; a_i, b_i, and c_i = the coefficients; and X, Y = the coordinates. The deviation of the actual displacement field from the linear least-squares approximation represents its relative nonlinearity. As a measure of this deviation, we define, for each particle in the packing, a coefficient ζ to be the normalized difference of the magnitude of displacement obtained from computer simulation $|\Delta u_i^n|$, and that given by the linear least-squares fit $|\overline{\Delta u_i}(X^n, Y^n)|$, such that for the nth particle

$$\zeta = 100 \frac{|\Delta u_i^n| - |\overline{\Delta u_i}(X^n, Y^n)|}{\overline{\Delta U}} \quad \ldots\ldots (18)$$

where

$$\overline{\Delta U} = \sqrt{\frac{1}{N} \sum_n \left(|\Delta u_i^n| - \frac{\sum_n |\Delta u_i^n|}{N} \right)^2} \quad \ldots\ldots (19)$$

where $|\Delta u_i|$ refers to the magnitude of Δu_i; and N = the total number of particles in the packing. Since ζ is a measure of the difference of the actual displacement field and its linear least-squares approximation, the average of

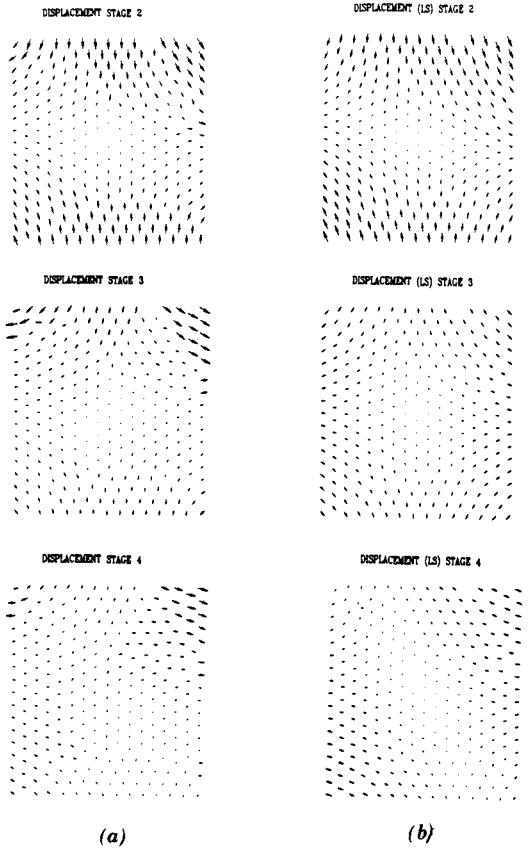

FIG. 4. Actual Displacement Fields and Linear Least-Square (LS) Approximation of Displacement Fields at Loading Stages 2, 3, and 4

ζ over all the particles is expected to be close to zero. The standard deviation of ζ over all the particles represents the relative disagreement of the actual displacement field with the linear least-squares approximation.

The displacement fields obtained from the computer simulation method for packing A with frictional contacts are shown in Fig. 4(*a*) at stages 2, 3, and 4. Since the displacements at stage 4 are large, the displacement fields in Fig. 4(*a*) are drawn at different scales. Fig. 4(*b*) shows the corresponding linear least-squares approximations of the displacement fields shown in Fig. 4(*a*). While in stage 2 [see Figs. 4(*a*) and (*b*)] the least-squares approximation agrees quite well with the displacement field from computer simulation, the agreement increasingly deteriorates for stages 3 and 4. To illustrate this deviation quantitatively, we plot in Fig. 5 the frequency distribution of coefficient ζ versus percentage of particles at four stages of loading [corresponding to 1-2-3-4 in Fig. 2(*b*)]. As the loading progresses, the distribution in Fig. 5 indicates an increase of standard deviation of coefficient ζ. The increasing standard deviation of ζ with the stress ratio signifies that uniform

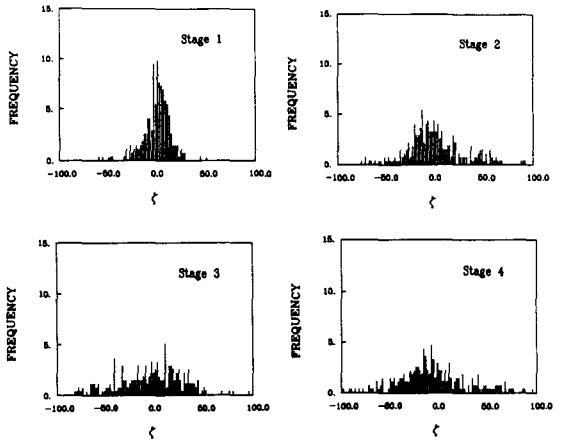

FIG. 5. Frequency Distribution of Displacement Variation Coefficient ζ at Loading Stages 1, 2, 3, and 4

strain is a poor representation at high stress ratios. In contrast, the displacement field obtained for the packings with bonded contacts is found to be fairly linear at all stress levels (Sharma 1989).

Particle Rotations

To show the heterogeneity of the particle rotation field, we plot in Fig. 6 the frequency distribution of particle rotations with percent-particles at stages 1 and 4 of the stress-strain curve for packing A with frictional contacts. From Fig. 6 it can be seen that the mean particle rotation is almost zero at the all stages of loading. This result is expected, because the stress axis coincides with the material axis, as can be seen from the contact normal distribution shown in Fig. 3. However, from Fig. 6 it is seen that the standard deviation of the particle rotations increases slightly with stress level. The increase in the standard deviation indicates an increase in the heterogeneity of the rotation field with stress level.

For packing A with bonded contacts under the same loading condition, the mean particle rotation is found, as expected, to be negligibly small from computer simulation and micro-structural continuum methods. Bathurst and Rothenburg (1988) have suggested that the contribution of rotation is rela-

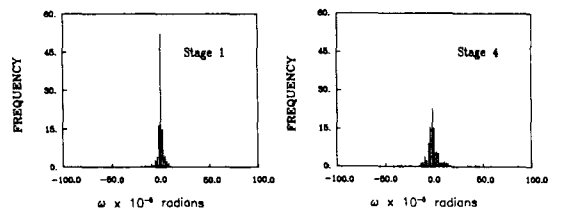

FIG. 6. Frequency Distribution of Particle Rotations ω at Loading Stages 1 and 4

tively small for dense packings (coordination number in range of 4 to 6) with linear contact interactions. The coordination number of the packing A is 5.1.

Stress in Packing

To investigate the heterogeneity of the stress field, we study the deviation of the stress for each particle. The stress associated with each particle can be computed from the contact forces as

$$\Delta\sigma_{ij}^{n} = \frac{1}{V_s(1+e)} \sum_{c} r_i^c \Delta f_j^c \quad \ldots\ldots (20)$$

where V_s = the area of the particle; e = the void ratio of the packing; r_i^c = the vector joining the centroid of a particle to the contact c; and Δf_j^c = the force acting at that contact. It can be easily shown that the mean stress defined in Eq. 13 is same as the average of particle stresses given by

$$\Delta\sigma_{ij} = \frac{1}{V} \sum_{n} V_s(1+e)\Delta\sigma_{ij}^{n} \quad \ldots\ldots (21)$$

We define Λ_{ij}^{n} to be the deviation of the particle stress $\Delta\sigma_{ij}^{n}$ from the mean stress $\Delta\sigma_{ij}$, that is

$$\Lambda_{ij}^{n} = \frac{\Delta\sigma_{ij}^{n} - \Delta\sigma_{ij}}{\Delta\sigma_{mm}} \quad \ldots\ldots (22)$$

In Fig. 7, the frequency distribution of three components of Λ_{ij}^{n} (for the 2-d case), are plotted with the percentage of particles for loading steps 1 and 4 for packing A with frictional contacts. The spread in the distribution indicates the inhomogeneity of the stress field. As expected, the stress field becomes increasingly heterogeneous with loading. Thus, though the mean stress may provide a good estimate of the overall stress in packing, higher moments of stress may be needed to capture the inhomogeneity accurately. Another interesting observation from this result is the presence of shear stresses at particles even though the mean shear stress is zero. Moreover, the magnitude of particle shear stresses increases with the loading.

Contact Forces

To illustrate the heterogeneity of the contact forces in the packing, we introduce coefficient ρ as the ratio of shear force to the Coulomb friction strength at the contact, where

$$\rho = \frac{f_s}{f_n \tan\phi_\mu} \text{ (for frictional contacts);}$$

$$\text{and} \qquad \rho = \frac{f_s}{f_n} \text{ (for bonded contacts)} \quad \ldots\ldots (23)$$

where f_s and f_n = the shear and normal force at the contact respectively; and ϕ_μ = the contact friction angle. The ratio ρ will take a positive or negative sign based on the orientation of the contact normal and the choice of the local coordinate system. The sign convention chosen here is illustrated schematically in Fig. 8. The local coordinate system is chosen to consist of two

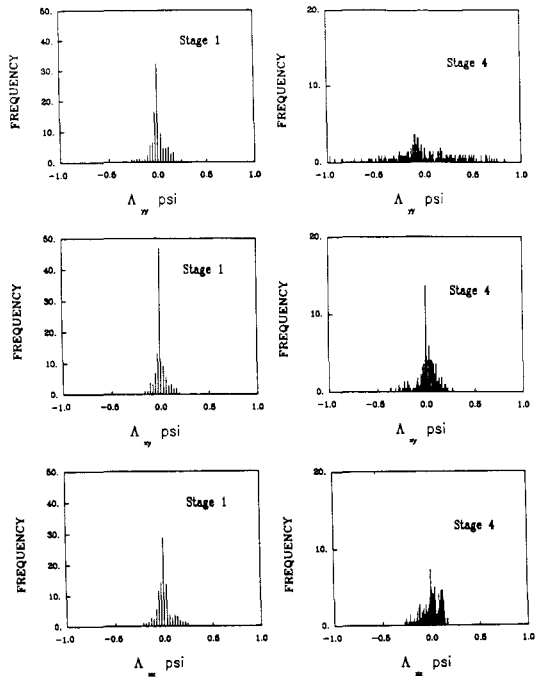

FIG. 7. Frequency Distribution of Stress Variation Coefficients Λ_{xx}, Λ_{xy}, and Λ_{yy} at Loading Stages 1 and 4

orthogonal vectors **n** and **s**, where **n** is the outward normal vector at the contact and the direction of **s** is chosen to follow the right-hand rule. Shear force in positive **s**-direction is taken to be positive. For example, for a contact normal in the first quadrant of the global coordinate system (particles m and n on the right side of Fig. 8) and for compressive loading in the Y-direction, the relative movement between the particles will be such that shear force is negative.

When the contact shear force equals the Coulomb friction strength, the

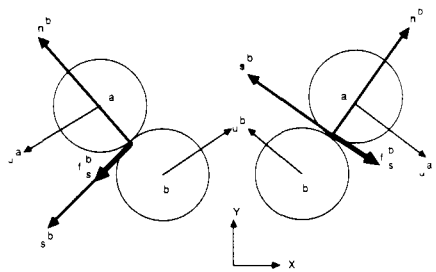

FIG. 8. Schematic Diagram to Illustrate Sign Convention of Contact Force Ratio ρ in Figs. 9 and 10

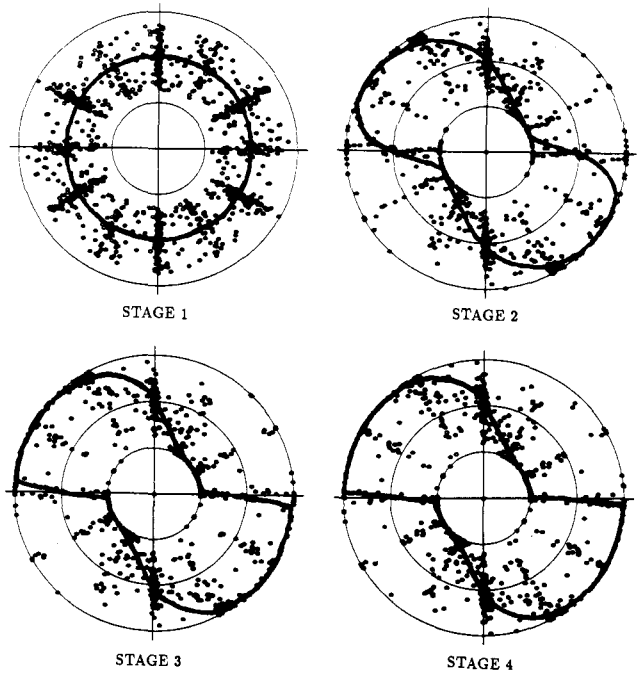

FIG. 9. Distribution of Contact Force Ratio ρ at Loading Stages 1, 2, 3, and 4 for Packing A with Frictional Contacts

ratio ρ takes the value of +1 or −1. The outer circle in Fig. 9 represents the value of ρ = +1 and the inner circle takes the value of ρ = −1. The circle in the center represents contacts with zero shear force. Fig. 9 shows the plot of spatial distribution of ρ for the loading stages 1–4 for packing A with frictional contacts. The distribution obtained from computer simulation is shown by symbols and the distribution from the micro-structural continuum model is shown by a continuous line. The general trend of distribution of ρ is similar for both methods; however, large scatter is observed in the computer simulation method. The micro-structural continuum model does not capture the variation in the local behavior. The results show the presence of distinct ranges of orientations along which the contacts are sliding.

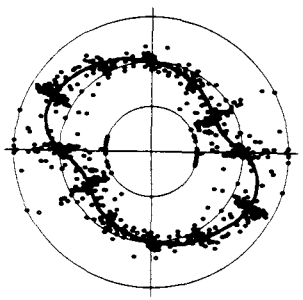

FIG. 10. Distribution of Contact Force Ratio ρ at Loading Stages 3 for Packing A with Bonded Contacts

For packing A with bonded contact, the contact force ratio ρ defined in Eq. 23 can be greater than 1. In the case of bonded contacts, it is found that the scatter of the contact force ratio is lower than that of the frictional contacts as shown in Fig. 10 for the stage 3 of the stress-strain curve.

Conclusions

The results of computer simulation on packing of disks shows that the type of contact interaction significantly affects the homogeneity of the various micro- and macro-mechanical measures in heterogeneous granular solids. For granular solids with bonded contacts, the strain field is found to be relatively homogeneous. For granular solids with frictional contacts, the results show that the strain field is homogeneous at low stress levels but becomes increasingly heterogeneous at high stress levels. This implies that the micro-structural continuum model based on uniform strain theory is applicable to packings with bonded contacts, such as for obtaining the moduli of cemented sands and sintered materials. The model is also applicable to packings with frictional contacts at low stress levels, such as for obtaining the initial moduli in low-amplitude vibration problems in granular soils.

However, the micro-structural continuum model gives a large discrepancy for packings with nonlinear frictional contacts at high stress levels even with the incorporation of packing evolution and particle rotation. This discrepancy is primarily due to the heterogeneity of the strain field. To model behavior of frictional granular media based on a micro-structural continuum approach at high levels of deviatoric stress, such as near failure, it is necessary to account for the heterogeneity in the strain field.

Appendix I. Contact Stiffness and Governing Equations for Computer Simulation

The normal and the tangential stiffness at contacts are based on the Hertz-Mindlin theory of frictional contacts (Mindlin 1949) considering partial slip at the contacts.

Two-Disk System

The normal and tangential contact stiffness are given by

$$K_n = \frac{1 - \nu_g}{\pi G_g}\left[2 \ln\left(\frac{2r}{A}\right) - 1\right] \quad \ldots\ldots (24)$$

$$K_s = C_2 K_n \left(1 - \frac{f_s}{f_n \tan \phi_\mu}\right)^{1/2} \quad \ldots\ldots (25)$$

where

$$A = \left[\frac{2r(1 - \nu_g) f_n}{\pi G_g}\right]^{1/2} \quad \ldots\ldots (26)$$

$$\frac{1}{r} = \frac{1}{2}\left(\frac{1}{r_1} + \frac{1}{r_2}\right) \quad (27)$$

where r_1 and r_2 = the radii of the contiguous disks; f_n = the magnitude of the normal force at the contact; f_s = the resultant tangential force at the contact; G_g and ν_g = the shear modulus and Poisson's ratio of the particle; C_2 = a material constant; and ϕ_μ = particle-to-particle friction angle.

Two Sphere System

The normal and tangential contact stiffness are given by

$$K_n = C_1 f_n^\alpha \quad (28)$$

$$K_s = C_2 K_n \left(1 - \frac{f_s}{f_n \tan \phi_\mu}\right)^{1/3} \quad (29)$$

where

$$C_1 = \left[\frac{3rG_g^2}{(1-\nu_g)^2}\right]^{1/3} \quad (30)$$

$$C_2 = \frac{2(1-\nu_g)}{2-\nu_g} \quad (31)$$

and $\alpha = 1/3$.

Several methods of computer simulation of granular materials have been used (Cundall and Strack 1979; Serrano and Rodriguez-Ortiz 1973; Kishino 1987). While the method by Cundall and Strack treats the problem as a dynamical one, the other two methods approach it from a statical point of view. In this work, since the focus is on a small deformation problem under quasi-static conditions, we use an approach analogous to that by Serrano and Rodriguez-Ortiz.

Considering the equilibrium condition for the mth particle in the packing and using Eqs. 1, 2, 3, and 5, we obtain the following governing equations for the computer simulation:

$$\Delta F_i^m = \sum_\alpha K_{ij}^{m\alpha}[\Delta u_j^m - \Delta u_j^n + e_{jkl}(\Delta\omega_k^m r_l^{m\alpha} - \Delta\omega_k^n r_l^{n\alpha})] = \sum_\alpha f_i^{m\alpha} \quad (32)$$

and

$$\Delta M_i^m = \sum_\alpha e_{ijl} K_{jk}^{m\alpha}[\Delta u_k^m - \Delta u_k^n + e_{kpq}(\Delta\omega_p^m r_q^{m\alpha} - \Delta\omega_p^n r_q^{n\alpha})] r_l^{m\alpha}$$

$$+ G_{ij}^{m\alpha}[\Delta\omega_j^m - \Delta\omega_j^n] = \sum_\alpha e_{ijl} f_j^{m\alpha} r_l^{m\alpha} + \mu_i^{m\alpha} \quad (33)$$

where m and n = the particles in contact at the αth contact; ΔF_i^m = the force; ΔM_i^m = the moment acting at the centroid of the mth particle; $f_i^{m\alpha}$ = the force; and $\mu_i^{m\alpha}$ = the moment acting on the αth contact of the mth particle. For those particles on which no external load is acting, $F_i^m = 0$ and $M_i^m = 0$. Eqs. 32 and 33 represent $6M$ equations in terms of $3M$ particle forces, $3M$ particle moments, $3M$ particle displacements, and $3M$ particle rotations for an assembly of M particles. If $3M$ of the variables are known, the system is determinate and the equations can be solved simultaneously to obtain the unknowns. The unknowns can either be the particle movements or the particle forces or a mixture of the two. To account for the nonlinear contact, the computations are carried out incrementally with iterations within each increment in the same manner as those in the initial stress algorithms of finite element methods for nonlinear material behavior (Zienkiewicz 1977). Within each increment, the sliding at the contact and the separation between particles are checked and accounted. The coordinates of the disk centers are updated at the end of each increment.

Appendix II. References

Bathurst, R. J., and Rothenburg, L. (1988). "Micromechanical aspects of isotropic granular assemblies with linear contact interactions." *J. Appl. Mech.*, 55(1), 17–23.

Chang, C. S. (1987). "Micromechanical modelling of constitutive relations for granular material." *Micromechanics of Granular Materials*, M. Satake and J. T. Jenkins, eds., Elsevier, Amsterdam, The Netherlands, 271–278.

Chang, C. S., and Misra, A. (1989a). "Theoretical and experimental study of regular packings of granules." *J. Engrg. Mech.*, ASCE, 115(4), 704–720.

Chang, C. S., and Misra, A. (1989b). "Computer simulation and modelling of mechanical properties of particulates." *Computers and Geotech.*, 7(4), 269–287.

Christoffersen, J., Mehrabadi, M. M., and Nemat-Nasser, S. (1981). "A micromechanical description of granular material behavior." *J. Appl. Mech.*, 48(2), 339–344.

Cowin, S. C., and Satake, M. (1978). *Continuum mechanical and statistical approaches in the mechanics of granular materials*, Gakujutsu Bunken Fukyukai, Tokyo, Japan.

Cundall, P. A., and Strack, O. D. L. (1979). "A discrete numerical model for granular assemblies." *Geotechnique*, 29(1), 47–65.

Digby, P. J. (1981). "The effective elastic moduli of porous granular rocks." *J. Appl. Mech.*, 48(4), 803–808.

Drescher, A., and deJosselin deJong, G. (1972). "Photoelastic verification of a mechanical model for the flow of a granular material." *J. Mech. and Physics of Solids*, 20(2), 337–351.

Jenkins, J. T., and Satake, M. (1983). *Mechanics of granular materials: New models and constitutive relations*. Elsevier, New York, N.Y.

Jenkins, J. T. (1987). "Volume change in small strain axisymmetric deformations of a granular material." *Micromechanics of Granular Materials*, M. Satake and J. T. Jenkins, eds., Elsevier, Amsterdam, The Netherlands, 245–252.

Kishino, Y. (1987). "Discrete model analysis of granular media." *Micromechanics of Granular Materials*, M. Satake and J. T. Jenkins, eds., Elsevier, Amsterdam, The Netherlands, 143–152.

Mindlin, R. D. (1949). "Compliance of elastic bodies in contact." *J. Appl. Mech.*, 16(3), 259–268.

Mindlin, R. D., and Deresiewicz, H. (1953). "Elastic spheres in contact under varying oblique forces." *J. Appl. Mech.*, 20(3), 327–344.

Oda, M. (1972). "Deformational mechanism of sand in triaxial compression tests." *Soils and Foundations*, 12(4), 1–18.

Oda, M., Nemat-Nasser, S., and Mehrabadi, M. (1982). "A statistical study of fabric in a random assembly of spherical granules." *Int. J. Numerical and Analytical Methods in Geomech.*, 6(1), 77–94.

Roscoe, K. H. (1970). "The influence of strains in soil mechanics." *Geotechnique*, 20(2), 129–170.

Satake, M., and Jenkins, J. T. (1989). *Micromechanics of granular materials*. Elsevier, New York, N.Y.

Serrano, A. A., and Rodriguez-Ortiz, J. M. (1973). "A contribution to the mechanics of heterogeneous granular media." *Proc., Symp. on Plasticity and Soil Mech.*, Cambridge, England.

Sharma, M. (1989). "Results from computer simulation of disk packings with linear contacts." *Report No. OUR-89-01/UMASS,* Univ. of Massachusetts, Amherst, Mass.
Walton, K. (1987). "The effective elastic moduli of a random packing of spheres." *J. Mech. and Physics of Solids,* 35(2), 213–226.
Xue, J. H. (1988). "Experimental studies on mechanical behavior of idealized granular media." Thesis submitted to the Univ. of Massachusetts, at Amherst, Mass., in partial fulfillment of the requirements of the degree of Master of Science.
Zienkiewicz, O. C. (1977). *The finite element method.* McGraw-Hill Book Co., London, U.K.

APPENDIX III. NOTATION

The following symbols are used in this paper:

C_{ijkl} = constitutive tensor;
e_{ijk} = permutation symbol;
Δf_i = contact force;
G_{ij} = contact rotational stiffness;
K_{ij} = contact stiffness;
l_i = branch vector;
Δu_i = particle displacement;
V = volume of the packing;
$\Delta\delta_i$ = relative displacement between particles;
$\Delta\epsilon_{ij}$ = strain tensor;
$\Delta\mu_i$ = contact moment;
$\Delta\omega_i$ = particle rotation;
$\Delta\sigma_{ij}$ = stress tensor; and
$\Delta\theta_i$ = relative rotation between particles.